



Detailed Balance and Exact Results for Density Fluctuations in Supersonic Turbulence

Liubin Pan¹, Paolo Padoan^{2,3} , and Åke Nordlund⁴¹ School of Physics and Astronomy, Sun Yat-sen University, 2 Daxue Road, Zhuhai, Guangdong, 519082, People's Republic of China; panlb5@mail.sysu.edu.cn² Institut de Ciències del Cosmos, Universitat de Barcelona, IEEC-UB, Martí Franquès 1, E-08028 Barcelona, Spain; ppadoan@icc.ub.edu³ ICREA, Pg. Lluís Companys 23, E-08010 Barcelona, Spain⁴ Centre for Star and Planet Formation, Niels Bohr Institute and Natural History Museum of Denmark, University of Copenhagen, Øster Voldgade 5-7, DK-1350 Copenhagen K, Denmark; aake@nbi.ku.dk

Received 2018 August 24; revised 2018 September 28; accepted 2018 September 30; published 2018 October 12

Abstract

The probabilistic approach to turbulence is applied to investigate density fluctuations in supersonic turbulence. We derive kinetic equations for the probability distribution function (PDF) of the logarithm of the density field, s , in compressible turbulence in two forms: a first-order partial differential equation involving the average divergence conditioned on the flow density, $\langle \nabla \cdot \mathbf{u} | s \rangle$, and a Fokker–Planck equation with the drift and diffusion coefficients equal to $-\langle \mathbf{u} \cdot \nabla s | s \rangle$ and $\langle \mathbf{u} \cdot \nabla s | s \rangle$, respectively. Assuming statistical homogeneity only, the detailed balance at steady state leads to two exact results, $\langle \nabla \cdot \mathbf{u} | s \rangle = 0$, and $\langle \mathbf{u} \cdot \nabla s | s \rangle = 0$. The former indicates a balance of the flow divergence over all expanding and contracting regions at each given density. The exact results provide an objective criterion to judge the accuracy of numerical codes with respect to the density statistics in supersonic turbulence. We also present a method to estimate the effective numerical diffusion as a function of the flow density and discuss its effects on the shape of the density PDF.

Key words: ISM: kinematics and dynamics – stars: formation – turbulence

1. Introduction

Supersonic turbulence in molecular clouds plays a crucial role in the process of star formation. The probability distribution function (PDF) of density fluctuations in supersonic turbulence has been extensively investigated (e.g., Vazquez-Semadeni 1994; Padoan et al. 1997; Nordlund & Padoan 1999; Molina et al. 2012) and widely used in theoretical models of star formation (Krumholz & McKee 2005; Hennebelle & Chabrier 2011; Padoan & Nordlund 2011a; Federrath & Klessen 2012). In star formation models based on turbulent fragmentation, the shape of the density PDF, particularly its high-density tail, is of particular importance due to its impact on the star formation rate and the predicted stellar initial mass function (e.g., Padoan et al. 1997; Padoan & Nordlund 2002; Hennebelle & Chabrier 2008; Padoan & Nordlund 2011a, 2011b). Numerical simulations of isothermal supersonic turbulence with solenoidal forcing have shown that the density PDF is generally consistent with a lognormal distribution, whereas changes in the equation of state (Passot & Vázquez-Semadeni 1998; Scalo et al. 1998), the forcing pattern (Federrath et al. 2008, 2010), and the inclusion of gravity (Collins et al. 2011; Kritsuk et al. 2011) all induce variations in the PDF shape.

The density PDFs used in star formation models are usually based on results from numerical simulations. The theoretical understanding of the origin of such PDFs is still incomplete, with most interpretations of numerical results being heuristic or qualitative. For example, the usual argument that the lognormal distribution is the consequence of a multiplicative process of successive, independent compressions and expansions is purely phenomenological. Also, it is not clear how artificial numerical diffusion that exists in all simulations affects the PDF shape.

In this Letter, we study the density statistics from first principles, by deriving kinetic equations of the density PDF.

Exact results corresponding to the detailed balance of probability fluxes at steady state are derived using the assumption of statistical homogeneity only (Section 2). We stress that, due to strong nonlinearity, exact results in turbulence are very rare, with the known examples being Kolmogorov's celebrated 4/5 law and similar ones in different flow cases (e.g., Yaglom 1949; Politano & Pouquet 1998; Galtier & Banerjee 2011). The exact results are used to test the accuracy of numerical simulations in Section 3, and our conclusions are summarized in Section 4.

2. The PDF Equations and Exact Results

2.1. The PDF Equations

Defining the logarithm of the density, $s \equiv \ln(\rho/\langle \rho \rangle)$, with $\langle \rho \rangle$ the average density, the continuity equation reads

$$\frac{\partial s}{\partial t} + \mathbf{u} \cdot \nabla s = -\nabla \cdot \mathbf{u}, \quad (1)$$

where \mathbf{u} is the turbulent velocity. Following the general procedure of the probabilistic approach for turbulence studies (e.g., Pope 2000), we define a fine-grained PDF, $g(\zeta; \mathbf{x}, t) = \delta(\zeta - s(\mathbf{x}, t))$, where δ is the Dirac delta function and ζ the sampling variable. The time derivative of g is given by $\partial_t g(\zeta; \mathbf{x}, t) = -\partial_\zeta g \partial_t s$, as g depends on t only through $(\zeta - s(\mathbf{x}, t))$. Using Equation (1) for $\partial_t s$ yields

$$\frac{\partial g(\zeta; \mathbf{x}, t)}{\partial t} = \frac{\partial(g\mathbf{u} \cdot \nabla s)}{\partial \zeta} + \frac{\partial(g\nabla \cdot \mathbf{u})}{\partial \zeta}, \quad (2)$$

where the last two terms use the fact that $\nabla \cdot \mathbf{u}$ and $\mathbf{u} \cdot \nabla s$ are independent of the sampling variable, ζ .

The coarse-grained PDF is defined as the ensemble average of g , i.e., $f(\zeta; \mathbf{x}, t) \equiv \langle g(\zeta; \mathbf{x}, t) \rangle$, over independent flow

realizations. The ensemble average of the product of any quantity, $\phi(\mathbf{x}, t)$, with g (a delta function) can be written in terms of a conditional average, $\langle \phi(\mathbf{x}, t) \delta(\zeta - s(\mathbf{x}, t)) \rangle = \langle \phi(\mathbf{x}, t) | s(\mathbf{x}, t) = \zeta \rangle f(\zeta; \mathbf{x}, t)$, where $\langle \phi(\mathbf{x}, t) | s(\mathbf{x}, t) = \zeta \rangle$ is the average of ϕ over the realizations where $s(\mathbf{x}, t)$ equals the sampling variable (Pope 2000). Ensemble averaging Equation (2) then gives

$$\frac{\partial f(\zeta; \mathbf{x}, t)}{\partial t} = \frac{\partial}{\partial \zeta} (\langle \mathbf{u} \cdot \nabla s | s = \zeta \rangle f) + \frac{\partial}{\partial \zeta} (\langle \nabla \cdot \mathbf{u} | s = \zeta \rangle f), \quad (3)$$

where the last two terms represent the fluxes of probability into and out of a given s interval by the advection of s and the divergence, respectively. At steady state, a balance of the probability flux is expected. We refer to $\langle \nabla \cdot \mathbf{u} | s = \zeta \rangle$ and $\langle \mathbf{u} \cdot \nabla s | s = \zeta \rangle$, as the conditional mean divergence and conditional mean advection, respectively.

An important relation exists between the two conditional means. Ensemble averaging the equality $g \nabla \cdot \mathbf{u} = \nabla \cdot (g \mathbf{u}) - \mathbf{u} \cdot \nabla g = \nabla \cdot (g \mathbf{u}) + (\mathbf{u} \cdot \nabla s) \partial_\zeta g$, and assuming statistical homogeneity, we find that

$$\langle \nabla \cdot \mathbf{u} | s = \zeta \rangle f = \frac{\partial}{\partial \zeta} (\langle \mathbf{u} \cdot \nabla s | s = \zeta \rangle f). \quad (4)$$

Using this relation in Equation (3) leads to two forms of kinetic equations for $f(\zeta; \mathbf{x}, t)$, one of which is

$$\frac{\partial f}{\partial t} = \langle \nabla \cdot \mathbf{u} | s = \zeta \rangle f + \frac{\partial}{\partial \zeta} (\langle \nabla \cdot \mathbf{u} | s = \zeta \rangle f), \quad (5)$$

where the PDF evolution is determined by the conditional mean divergence. The other form is a Fokker–Planck equation,

$$\frac{\partial f}{\partial t} = \frac{\partial}{\partial \zeta} (\langle \mathbf{u} \cdot \nabla s | s = \zeta \rangle f) + \frac{\partial^2}{\partial \zeta^2} (\langle \mathbf{u} \cdot \nabla s | s = \zeta \rangle f), \quad (6)$$

where the drift and diffusion coefficients are $-\langle \mathbf{u} \cdot \nabla s | s = \zeta \rangle$ and $\langle \mathbf{u} \cdot \nabla s | s = \zeta \rangle$, respectively. The diffusion term in Equation (6) tends to broaden the PDF, while the drift term reduces the mean of s . By analyzing $\langle \mathbf{u} \cdot \nabla s | s = \zeta \rangle$, the Fokker–Planck equation may be conveniently used to study the development of density fluctuations and the evolution of the PDF from initial conditions.

Equations (5) and (6) for the PDF of s are exact; however, they are not closed (hence not directly solvable) because the conditional means involve two-point, density-velocity joint statistics, whose evolution relies on three-point joint statistics and so on. For simplicity, we will drop the sampling variable, ζ , and write the PDF as $f(s; t)$, and any conditional mean $\langle \dots | s = \zeta \rangle$ as $\langle \dots | s \rangle$.

2.2. Exact Results at Statistically Steady State

At statistically steady state, exact results corresponding to the balance of probability fluxes can be derived from the PDF equations. At steady state, Equation (5) is solved by $\langle \nabla \cdot \mathbf{u} | s \rangle f(s) = C \exp(-s)$, where C is the integration constant. The integral of $\langle \nabla \cdot \mathbf{u} | s \rangle f(s)$ from $-\infty$ to ∞ is $\langle \nabla \cdot \mathbf{u} \rangle$, which is zero from homogeneity. This requires $C = 0$, so that

$$\langle \nabla \cdot \mathbf{u} | s \rangle = 0, \quad (7)$$

for all s , indicating that, at each given density, the values of the velocity divergence in expanding and converging regions of a

compressible turbulent flow cancel out exactly. This exact balance at each density is a *detailed* version of the overall balance, $\langle \nabla \cdot \mathbf{u} \rangle = 0$, that follows simply from statistical homogeneity.

Combining Equations (7) and (4) gives $\langle \mathbf{u} \cdot \nabla s | s \rangle f = C_2$, with C_2 another integration constant. Considering that $\int_{-\infty}^{\infty} \langle \mathbf{u} \cdot \nabla s | s \rangle f(s) ds = \langle \mathbf{u} \cdot \nabla s \rangle$ and that $\langle \mathbf{u} \cdot \nabla s \rangle = 0$ at steady state (as can be seen by averaging Equation (1)), we have $C_2 = 0$ and

$$\langle \mathbf{u} \cdot \nabla s | s \rangle = 0, \quad (8)$$

for all s . Note that our main results, Equations (7) and (8), are derived exactly, with only assumptions of statistical homogeneity and stationarity.

Equations (7) and (8) indicate that the probability fluxes due to the advection and divergence terms in Equation (3) are perfectly balanced individually. This individual balance of each term is not required by Equation (3), which only demands an overall balance $\langle \mathbf{u} \cdot \nabla s | s \rangle + \langle \nabla \cdot \mathbf{u} | s \rangle = 0$ at steady state. It is the relation in Equation (4) that leads to individual balances of the two terms. We will refer to both Equation (7) and Equation (8) as detailed balance.

3. Simulation Results

3.1. Effects of Artificial Numerical Diffusion

The results derived in Section 2 are expected to hold exactly, as long as the assumed statistical homogeneity and stationarity are satisfied. However, the artificial numerical diffusion of the density field, which is unavoidable in simulations but absent in real flows, may cause departures from the exact results. As the continuity equation is evolved on a discrete grid, strictly speaking, the computed density field is not the exact solution. For example, the length scale of density structures is limited by the size of the computational cell, and intense structures such as shocks would appear more diffuse than in real flows. This effect of discretization is responsible for the departure of the simulation results from our exact relations, Equations (7) and (8), which may be used as a tool to evaluate the accuracy of the simulations.

The numerical diffusion in a specific simulation also depends on the adopted solver and the details of its implementation, such as the regularization methods used to stabilize the shocks. To examine the effects of numerical diffusion, we adopt a generic form, $\nabla \cdot (\kappa(\rho) \nabla \rho)$, where, for simplicity, the diffusivity $\kappa(\rho)$ is assumed to depend only on the density. This assumed form of the numerical diffusion gives a contribution of $\kappa(\nabla s)^2 + \nabla \cdot (\kappa \nabla s)$ to Equation (1), which leads to

$$\begin{aligned} \frac{\partial f(s; t)}{\partial t} &= \frac{\partial}{\partial s} (\langle \mathbf{u} \cdot \nabla s | s \rangle f - \kappa(s) \langle (\nabla s)^2 | s \rangle f) \\ &+ \frac{\partial^2}{\partial s^2} (\langle \mathbf{u} \cdot \nabla s | s \rangle f - \kappa(s) \langle (\nabla s)^2 | s \rangle f), \end{aligned} \quad (9)$$

which is again a Fokker–Planck equation. We will refer to $\kappa(s) \langle (\nabla s)^2 | s \rangle$ as the conditional mean dissipation of s . The drift and diffusion coefficients indicate a competition between the conditional mean advection and the numerical diffusion, which tend to broaden and narrow the PDF, respectively. At steady state, the two terms must cancel out, i.e., $\langle \mathbf{u} \cdot \nabla s | s \rangle = \kappa(s) \langle (\nabla s)^2 | s \rangle$, suggesting that the numerical diffusion of density tends to make the conditional mean advection positive rather than 0. The relation provides an

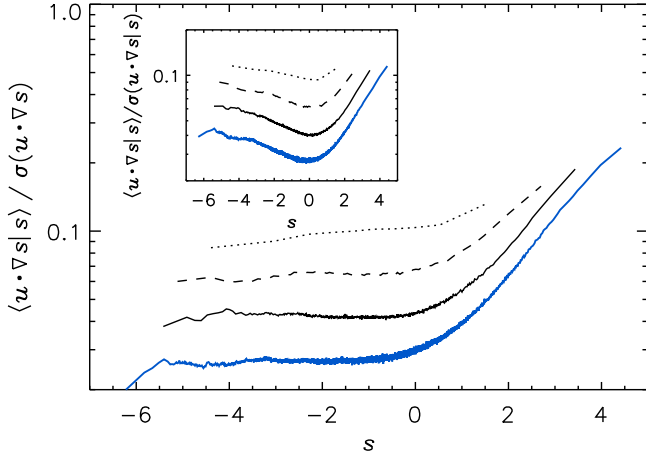


Figure 1. Conditional mean advection, $\langle \mathbf{u} \cdot \nabla s | s \rangle$, normalized to the rms, $\langle (\mathbf{u} \cdot \nabla s)^2 \rangle^{1/2}$, of the advection term. The inset shows the same quantity normalized to the conditional rms $\langle (\mathbf{u} \cdot \nabla s)^2 | s \rangle^{1/2}$ in each s bin. Dotted, dashed, solid, and blue solid lines show results at 128^3 , 256^3 , 512^3 , and 1024^3 resolution, respectively.

estimate of the effective numerical diffusivity as a function of s ,

$$\kappa(s) = \langle \mathbf{u} \cdot \nabla s | s \rangle / \langle (\nabla s)^2 | s \rangle. \quad (10)$$

The effect of numerical diffusion is expected to decrease with increasing resolution, so our exact results, Equations (7) and (8), should be better satisfied at higher resolution.

3.2. Comparison with Simulation Data

We simulated an isothermal, supersonic turbulent flow with rms Mach number ~ 7.5 , using the recently developed code *Dispatch* (Nordlund et al. 2018). We solved the 3D hydrodynamic equations without explicit viscosity in a periodic simulation box of unit size, using the Harten–Lax–van Leer–Contact (HLLC) approximate Riemann solver (Toro et al. 1994). The flow was driven with a solenoidal random force in Fourier space at wavenumbers $1 \leq 1/2\pi \leq 2$. The simulations lasted 15 dynamical times, and we used the last 30 snapshots covering 10 dynamical times for statistical analysis. In order to examine the dependence on numerical resolution, we carried out simulations at four resolutions, from 128^3 to 1024^3 . Note that our theoretical results are general, applicable to all compressible flows, and the specific choice of code and simulation here is intended only to show how to use our exact results to test the accuracy of simulations and to illustrate the method to estimate numerical diffusivity.

To compute the conditional statistics, we divide the s space into bins of different widths, such that the sample size of each bin is constant, $\simeq 6.3$ million. We first analyze the conditional mean advection at steady state. Figure 1 plots $\langle \mathbf{u} \cdot \nabla s | s \rangle$ at different resolutions. The main panel normalizes it to the overall rms advection in the entire flow. Our theory predicts that the conditional mean advection vanishes exactly. However, the existence of numerical diffusion causes $\langle \mathbf{u} \cdot \nabla s | s \rangle$ to be positive at all s , because it is in balance with the positive-definite conditional mean dissipation $\kappa(s) \langle (\nabla s)^2 | s \rangle$ at steady state (Section 3.1). Therefore, the departure of $\langle \mathbf{u} \cdot \nabla s | s \rangle$ from zero reflects the amplitude of numerical diffusion of density. Figure 1 shows that $\langle \mathbf{u} \cdot \nabla s | s \rangle$ is small and almost constant at small s , and then quickly rises at $s \gtrsim 1$, indicating an increase of the numerical dissipation with s .

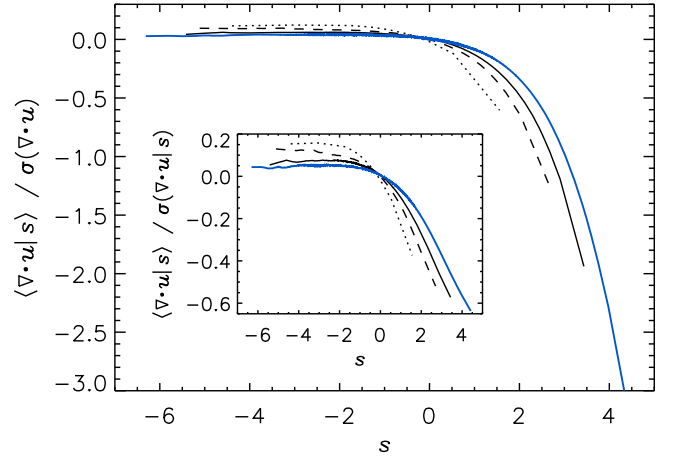


Figure 2. Conditional mean divergence, $\langle \nabla \cdot \mathbf{u} | s \rangle$, normalized to the overall rms flow divergence, $\langle (\nabla \cdot \mathbf{u})^2 \rangle^{1/2}$ (main panel), and to the conditional rms $\langle (\nabla \cdot \mathbf{u})^2 | s \rangle^{1/2}$ (inset) in each s bin.

The inset of Figure 1 shows the ratio of the conditional mean advection to the conditional rms, $\langle (\mathbf{u} \cdot \nabla s)^2 | s \rangle^{1/2}$, in each s bin. The ratio reflects how close to zero the conditional mean advection is. The ratio is much smaller than 1; it is only $\simeq 0.12$ at the lowest resolution, and decreases steadily with increasing resolution, to about 0.03 for small s at 1024^3 . This continuous decrease with increasing resolution, without any sign of convergence, is consistent with our theory that predicts $\langle \mathbf{u} \cdot \nabla s | s \rangle = 0$ in the absence of numerical diffusion, which can be achieved only toward infinite resolution.

In Figure 2, we plot the conditional mean divergence $\langle \nabla \cdot \mathbf{u} | s \rangle$ measured from the simulation data. When normalized to the overall rms divergence, $\langle (\nabla \cdot \mathbf{u})^2 \rangle^{1/2}$ (main panel), the conditional mean divergence is close to zero and almost constant at small s . It then starts decreasing at $s \simeq -1$, and finally becomes negative and deviates significantly from zero at the largest values of s . The conditional mean divergence was also predicted to be zero, and like the case of $\langle \mathbf{u} \cdot \nabla s | s \rangle$, its departure from zero at large s also corresponds to the effect of numerical diffusion (see below). Intuitively, strong shocks in a simulation may result in structures that are initially unresolved, with lower densities than expected, and thus their negative divergence is artificially assigned to relatively lower densities. This contributes to the negative mean divergence, $\langle \nabla \cdot \mathbf{u} | s \rangle$, at large s .

The inset of Figure 2 normalizes $\langle \nabla \cdot \mathbf{u} | s \rangle$ to the conditional rms, $\langle (\nabla \cdot \mathbf{u})^2 | s \rangle^{1/2}$, of the divergence. This normalization is a better indicator of how well the negative and positive parts of the divergence PDF, which is generally very broad, cancel out at each given density. Except at the largest values of s , where the conditional mean to rms ratio reaches $\simeq -0.6$, $\langle \nabla \cdot \mathbf{u} | s \rangle$ is significantly smaller than $\langle (\nabla \cdot \mathbf{u})^2 | s \rangle^{1/2}$, especially at high resolutions. For both normalizations, the conditional mean divergence gets closer to zero with increasing resolution, again with no sign of convergence at 1024^3 . It is thus likely that $\langle \nabla \cdot \mathbf{u} | s \rangle$ continues to approach zero as the resolution increases further, consistent with our prediction that, in the absence of numerical diffusion, the divergence is perfectly balanced at each density level.

To understand the significant departure of $\langle \nabla \cdot \mathbf{u} | s \rangle$ from zero at large s , we make use of Equation (4), which provides a relation between $\langle \nabla \cdot \mathbf{u} | s \rangle$ and $\langle \mathbf{u} \cdot \nabla s | s \rangle$. We rewrite the

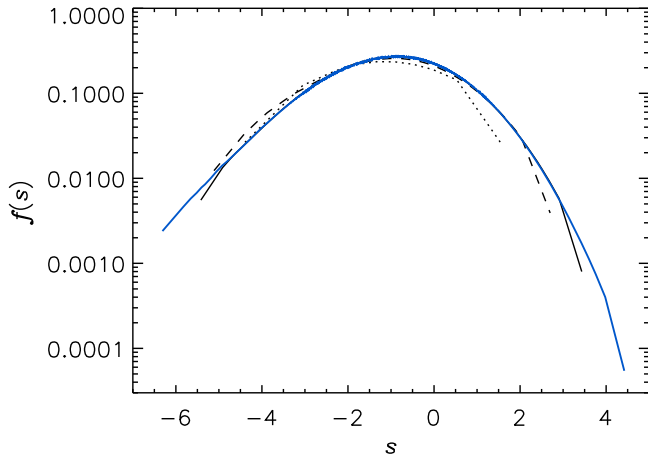


Figure 3. Probability distribution of s using the same s bins as for the analysis of the conditional means.

relation as $\langle \nabla \cdot \mathbf{u} | s \rangle = \partial_s \langle \mathbf{u} \cdot \nabla s | s \rangle + \langle \mathbf{u} \cdot \nabla s | s \rangle \partial_s [\ln f(s)]$. The second term, $\langle \mathbf{u} \cdot \nabla s | s \rangle \partial_s \ln f(s)$, is dominant at large s because the right tail of the density PDF, $f(s)$, decreases very fast (see Figure 3). Therefore, the decrease of $\langle \nabla \cdot \mathbf{u} | s \rangle$ below zero at large s corresponds to the decrease of $f(s)$ and the rise of $\langle \mathbf{u} \cdot \nabla s | s \rangle$ toward large densities. In particular, the fast decrease of $f(s)$ at large s explains why the departure of $\langle \nabla \cdot \mathbf{u} | s \rangle$ from zero is more significant than that of $\langle \mathbf{u} \cdot \nabla s | s \rangle$. The increase of $\langle \mathbf{u} \cdot \nabla s | s \rangle$ at large s is caused by numerical diffusion, therefore the significant departure of $\langle \nabla \cdot \mathbf{u} | s \rangle$ from zero at large s also reflects the effect of numerical diffusion. At small s ($s \lesssim -2$), both $\langle \nabla \cdot \mathbf{u} | s \rangle$ and $\langle \mathbf{u} \cdot \nabla s | s \rangle$ appear to be roughly constant (Figures 1 and 2). For constant $\langle \nabla \cdot \mathbf{u} | s \rangle$ and $\langle \mathbf{u} \cdot \nabla s | s \rangle$, Equation (4) implies that $f(s)$ is exponential, which is approximately consistent with the left PDF tail shown in Figure 3. However, the approximately exponential left tail is not expected in general, as its shape may depend on various factors, such as the flow Mach number, the driving pattern (Federrath et al. 2010), and possibly the numerical code.

We have found that, consistent with our theory, $\langle \nabla \cdot \mathbf{u} | s \rangle$ and $\langle \mathbf{u} \cdot \nabla s | s \rangle$ are close to zero at small s , and their departure from 0, occurring primarily at large s , reflects the artifacts of numerical diffusion and steadily decreases with increasing resolution.

Our analytical work provides a way to estimate the effective numerical diffusivity, $\kappa(s)$ (Equation (10)). As expected, Figure 4 shows the measured $\kappa(s)$ decreases with increasing resolution. For each factor of 2 increase in resolution, $\kappa(s)$ decreases by a factor of $\simeq 2$ for all s , and the shape of $\kappa(s)$ as a function of s appears to be independent of the resolution. The invariance is likely a result of the fact that Riemann solvers resolve shocks with a fixed number of cells, corresponding to a diffusivity that scales linearly with the cell size. Finite difference solvers with diffusivities proportional to the cell size are expected to show similar scaling behavior. If so, $\kappa(s)$ may be viewed as an intrinsic feature that characterizes each code. The invariance of the function form of $\kappa(s)$ with resolution in our simulation may be partly responsible for the convergence of the overall shape of the density PDF. As seen in Figure 3, the shape of $f(s)$ is also largely invariant with numerical resolution. The effect of increasing resolution is mainly to extend the PDF to a wider s range.

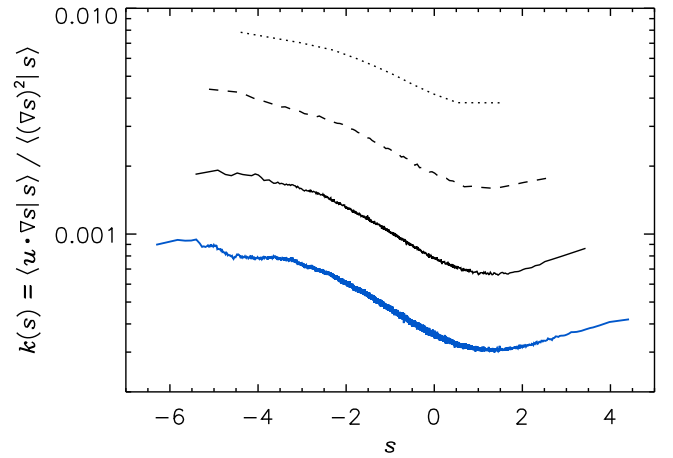


Figure 4. Measured numerical diffusivity, $\kappa(s)$, as a function of logarithmic density at different numerical resolutions.

At all resolutions, $\kappa(s)$ decreases by a factor of $\simeq 3$ as s increases to 1, and then slightly rises as s increases further. The decrease of $\kappa(s)$ with increasing s does not imply that the numerical dissipation, $\kappa(s) \langle (\nabla s)^2 | s \rangle$, is weaker at larger s . In fact, the larger departure from zero of $\langle \nabla \cdot \mathbf{u} | s \rangle$ and $\langle \mathbf{u} \cdot \nabla s | s \rangle$ at large s is due to the increase of the numerical dissipation of s toward large densities. Although $\kappa(s)$ at large s is already 2–3 times smaller than at small s , it is still not sufficient to keep the numerical dissipation of s in dense regions at a satisfactory level. Adopting adaptive-mesh-refinement methods could help further reduce the numerical diffusion at large s .

A fundamental question concerning density fluctuations in supersonic turbulence is how well the density PDF of a simulation represents the PDF, $f_{\text{real}}(s)$, of a real flow. The convergence of the PDF with resolution does not necessarily guarantee the PDF is accurate. Numerical diffusion is unavoidable in simulations, and its dependence on s may leave an artificial imprint on the density PDF. It is unknown what function form of $\kappa(s)$ would give density statistics closest to $f_{\text{real}}(s)$. Furthermore, if the function form of $\kappa(s)$ with s is invariant with resolution, as in our case, increasing resolution may not bring the shape of the PDF closer to f_{real} , as it may only extend the PDF to a wider density range. According to our preliminary results (L. Pan et al. 2018, in preparation), numerical diffusion in simulations may cause a significant underestimate of the high-density tail of the density PDF. A semi-analytical approach developed in our new work that removes the direct effect of the artificial diffusion of the density field predicts a power-law tail, while numerical simulations always yield a nearly lognormal tail.

Based on our exact results, we propose to use the departure from zero of the conditional means, $\langle \nabla \cdot \mathbf{u} | s \rangle$ and $\langle \mathbf{u} \cdot \nabla s | s \rangle$, at all values of s , as an objective criterion to evaluate the ability of numerical codes to reproduce the correct density PDF. This criterion will be adopted in the context of a future systematic study of the shape of the density PDF in turbulent flows simulated with different codes.

4. Conclusions

We have used both analytical and numerical approaches to investigate density fluctuations in compressible turbulence. Kinetic equations for the density PDF were derived in two

forms, a first-order partial differential equation (Equation (5)) and a Fokker–Planck equation (Equation (6)) with coefficients given by the conditional mean divergence, $\langle \nabla \cdot \mathbf{u} | s \rangle$, and advection, $\langle \mathbf{u} \cdot \nabla s | s \rangle$, respectively. With the assumption of statistical homogeneity only, two exact results were predicted, $\langle \nabla \cdot \mathbf{u} | s \rangle = 0$ and $\langle \mathbf{u} \cdot \nabla s | s \rangle = 0$, corresponding to the detailed balance of probability fluxes at steady state. In simulations, the departure of the conditional mean divergence and advection from zero corresponds to the artifacts of the numerical diffusion of the density field. Our exact results provide an objective measure for the accuracy of the density PDF from numerical simulations, suggesting that the codes yielding smaller departure of $\langle \nabla \cdot \mathbf{u} | s \rangle$ and $\langle \mathbf{u} \cdot \nabla s | s \rangle$ from zero are to be considered more accurate. A general method is also developed to measure the numerical diffusivity, $\kappa(s)$, as a function of s , which may be used to characterize each numerical code. A systematic study of the effects of numerical diffusion on the PDF shape using different codes is being planned and will be reported in future work.

L.P. acknowledges support from the Youth Program of the Thousand Talents Plan in China. P.P. acknowledges support by the Spanish MINECO under project AYA2017-88754-P (AEI/FEDER,UE). The work of Á.N. was supported by grant 1323-00199B from the Danish Council for Independent Research (DFF). The Centre for Star and Planet Formation is funded by the Danish National Research Foundation (DNRF97). Storage and computing resources at the University of Copenhagen HPC centre, funded in part by Villum Fonden (VKR023406), were used to carry out the simulations.

ORCID iDs

Paolo Padoan  <https://orcid.org/0000-0002-5055-5800>

References

- Collins, D. C., Padoan, P., Norman, M. L., & Xu, H. 2011, *ApJ*, 731, 59
- Federrath, C., & Klessen, R. S. 2012, *ApJ*, 761, 156
- Federrath, C., Klessen, R. S., & Schmidt, W. 2008, *ApJL*, 688, L79
- Federrath, C., Roman-Duval, J., Klessen, R. S., Schmidt, W., & Mac Low, M.-M. 2010, *A&A*, 512, A81
- Galtier, S., & Banerjee, S. 2011, *PhRvL*, 107, 134501
- Hennebelle, P., & Chabrier, G. 2008, *ApJ*, 684, 395
- Hennebelle, P., & Chabrier, G. 2011, *ApJL*, 743, L29
- Kritsuk, A. G., Norman, M. L., & Wagner, R. 2011, *ApJL*, 727, L20
- Krumholz, M. R., & McKee, C. F. 2005, *ApJ*, 630, 250
- Molina, F. Z., Glover, S. C. O., Federrath, C., & Klessen, R. S. 2012, *MNRAS*, 423, 2680
- Nordlund, Å., Ramsey, J. P., Popovas, A., & Küffmeier, M. 2018, *MNRAS*, 477, 624
- Nordlund, Å. K., & Padoan, P. 1999, in Proc. of 2nd Guillermo Haro Conference, Interstellar Turbulence, ed. J. Franco & A. Carraminana (Cambridge: Cambridge Univ. Press), 218
- Padoan, P., & Nordlund, Å. 2002, *ApJ*, 576, 870
- Padoan, P., & Nordlund, Å. 2011a, *ApJ*, 730, 40
- Padoan, P., & Nordlund, Å. 2011b, *ApJL*, 741, L22
- Padoan, P., Nordlund, A., & Jones, B. J. T. 1997, *MNRAS*, 288, 145
- Passot, T., & Vázquez-Semadeni, E. 1998, *PhRvE*, 58, 4501
- Politano, H., & Pouquet, A. 1998, *PhRvE*, 57, R21
- Pope, S. B. 2000, in Turbulent Flows, ed. B. P. Stephen (Cambridge: Cambridge Univ. Press), 806
- Scalo, J., Vázquez-Semadeni, E., Chappell, D., & Passot, T. 1998, *ApJ*, 504, 835
- Toro, E. F., Spruce, M., & Speares, W. 1994, *ShWav*, 4, 25
- Vázquez-Semadeni, E. 1994, *ApJ*, 423, 681
- Yaglom, A. M. 1949, Dokl. Akad. Nauk SSSR, 69, 6